forests

MDPI

Article

Features of Radial Growth Rate of Trees in Agro-Pastoral Transition Zone, Northern China

Jiayu Sun [1], Na Liu [1,2,*], Guang Bao [1,2,*], Yanchao Wang [3] and Qi Chu [1]

[1] Shaanxi Key Laboratory of Disaster Monitoring and Mechanism Simulating, College of Geography and Environment, Baoji University of Arts and Sciences, Baoji 721013, China
[2] State Key Laboratory of Loess and Quaternary Geology, Institute of Earth Environment, Chinese Academy of Sciences, Xi'an 710061, China
[3] College of Bioscience and Engineering, Xingtai University, Xingtai 054001, China
* Correspondence: liuna@bjwlxy.edu.cn (N.L.); baoguang@bjwlxy.edu.cn or baoguang23@163.com (G.B.)

Abstract: The Vaganov–Shashkin process-based model was used to explore the variation characteristic of the radial growth rate of *Pinus tabulaeformis* in the agro-pastoral transition zone in northern China. The tree-ring width chronologies of the four sampling sites were significantly positively correlated with the simulated series ($p < 0.01$), and the simulated onset and end dates of tree radial growth indicated that April to October was the main growing season. Temperature affects the radial growth rate of tree stems at the start and end of the growing season, while soil moisture availability affects the radial growth rate in the main growing season. Despite the differences in amplitude, the integral growth rate showed a bimodal pattern, which to some extent responded to the hydrothermal configuration of the East Asian summer monsoon climate. Compared with the peak changes in the summer monsoon fringe area in Northwest China, the highest peak of the integral growth rate in this study area appeared around August in the late growing season, reflecting the adaptability of trees to the local climatic environment. The average values of the integral growth rate and rate due to soil moisture, inferred from extreme wide-ring and narrow-ring years, were significantly different ($p < 0.01$), while the average growth rates due to temperature were not significant ($p > 0.05$). The analysis results indicate that moisture availability is a key limiting factor for the radial growth of *Pinus tabulaeformis*. Our study provides valuable knowledge about the growth processes of the main tree species related to the hydroclimatic variables in northern China and offers a new perspective on mitigating the adverse effects of a warmer climate on the forest in the semi-arid region in the future.

Keywords: Vaganov–Shashkin model; tree rings; agro-pastoral transition zone; East Asian summer monsoon; *Pinus tabulaeformis*

Citation: Sun, J.; Liu, N.; Bao, G.; Wang, Y.; Chu, Q. Features of Radial Growth Rate of Trees in Agro-Pastoral Transition Zone, Northern China. *Forests* **2022**, *13*, 1712. https://doi.org/10.3390/f13101712

Academic Editor: Jarosław Socha

Received: 17 September 2022
Accepted: 14 October 2022
Published: 17 October 2022

1. Introduction

As an important part of the terrestrial ecosystem, forests play a pivotal role in achieving sustainable economic and social development and maintaining harmony between human beings and the ecological environment due to functions such as climate regulation, carbon sequestration, and biodiversity conservation [1]. The negative effects of climate warming have already emerged [2,3]. Extreme climate events such as high temperature and drought have exacerbated forest decline and the risk of tree survival [4–7], leading to reduced forest net primary productivity (NPP) related to tree mortality [8,9]. Although increasing temperature contributes to an increase in forest NPP in high-latitude or alpine regions [10], the potential evapotranspiration and soil moisture deficits caused by warming could lead to possible negative impacts on tropical forest NPP [11], therefore resulting in a decreased NPP of the global terrestrial ecosystem [12]. The ecosystems of the arid–humid transition zone in northern China would encounter

severe challenges of high risk by the end of the 21st century under the future emission scenarios [13]. The NPP loss and risk over the eastern plain of North China and the southeastern grassland of Mongolian Plateau tend to intensify under the higher emission scenarios of the representative concentration pathways (RCPs) in the future [14]. The northern agro-pastoral transition zone is in the range of the arid–humid region [15]. It is also located in the East Asian summer monsoon edge, a region that is sensitive to climate fluctuations [16]. Large-scale forest mortality events tend to occur in the cold-temperature zone associated with high temperature and drought stress [17]. Therefore, tree growth in the agro-pastoral transition zone determines the stability of the forest and grassland landscape and the safety of the regional ecological environment. *Pinus tabulaeformis* is the main coniferous tree species in northern China and plays an important role in maintaining ecosystem health and stability. At the same time, it is a critical tree species for dendroclimatology research [18]. However, compared with the effects of monthly climatic factors on tree growth, exploring the physiological procession and effects of extreme weather and climate events on tree radial growth at the microscale is of great significance for the management of natural pine forests and for applying reasonable measures against climate change.

Simulations of the response characteristics of tree radial growth and hydroclimate factors based on physiological models have been widely carried out [19,20]. Among them, simulation studies conducted in China are mainly in the Tibetan Plateau [21] and northwest regions [22–25]. Compared with the studies of the growth rate variation of *P. tabulaeformis* on the daily scale in the northwestern edge of the East Asian summer monsoon area (Figure 1), related research on the northern part of the East Asian summer monsoon area has not yet been reported. The simulation studies of the radial growth of *P. tabulaeformis* based on the VS model will be helpful to further understand the climatic growth response characteristics of this major native tree species at different environment sites and provide scientific support for evaluating the health status and environmental adaptability of pine forests.

The objectives of this study are to (1) explore the ability of the Vaganov–Shashkin process-based model (VS model) to simulate the radial growth rates of *P. tabulaeformis* in northern China, (2) reveal the limiting factors of trees during the growing season at different sites, and (3) investigate the response differences in the radial growth of trees to climate factors at extremely wide and narrow growth rings during the past several decades.

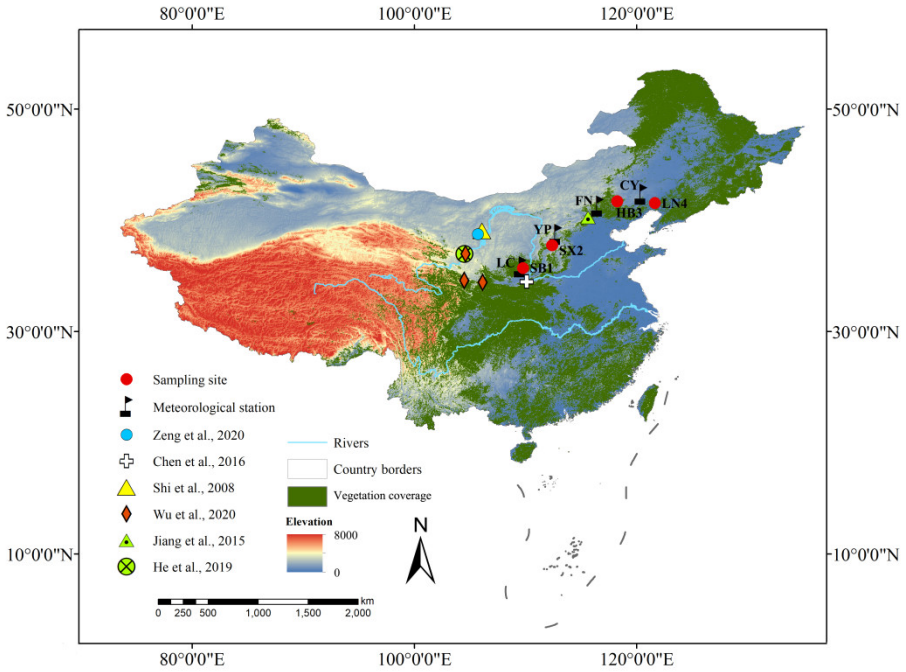

Figure 1. Locations of *Pinus tabulaeformis* tree-ring sampling sites (red dots: SB1, SX2, HB3, and LN4), meteorological stations (black flags: LC, YP, FN, and CY), and other sites marked by different symbols mentioned in this study.

2. Materials and Methods

2.1. Study Area and Tree-Ring Data

The temperature in northern China has increased significantly over the past few decades under the background of global warming [26]. Affected by the East Asian monsoon, the precipitation variability in this region is large, and it is one of the regions that is very sensitive to climate change [16]. The study areas were located in a transitional zone between the agricultural and pasture land, including the sampling sites of SB1 (35°33′ N–35°48′ N, 109°41′ E–109°49′ E, elevation 1134–1320 m) [27] and SX2 (37°44′ N, 112°22′ E, elevation 1255–1402 m) [28] in the Loess Plateau and two sites of HB3 (41°42′ N, 117°04′ E, elevation 966 m) [29] and LN4 (41°33′ N, 120°27′ E, elevation 169.6 m) [30] in the southeastern Mongolian Plateau (Figure 1). The site of SB1 is situated on Huanglong Mountain in the southeast of the Loess Plateau [27]. SX2 is located in the Tianlong Mountain Reserve in the middle section of the Fenhe River basin in the eastern Loess Plateau. The forest ecosystem is dominated by a coniferous mixed forest, including *P. tabulaeformis* [28]. HB3 lies in the intersection of Yinshan Mountain and Yanshan Mountain. It belongs to the transition zone from temperate grassland and coniferous forest to a warm, temperate, deciduous, broad-leaved forest, and drought occurs frequently in spring and summer [29]. The site of LN4 is located in the southern part of the Horqin Sandy Land, with an arid climate, poor soil, and a fragile ecological environment, which is a typical temperate continental monsoon climate [30].

The species used in this research is *P. tabulaeformis*, which is the main tree species for dendrochronological studies in northern China and is widely used in the reconstruction of regional hydroclimate change [18,31]. The sample sizes of each site are as follows: 54 cores/27 trees for SB1, 52 cores/25 trees for SX2, 47 cores/22 trees for HB3, and 31 cores/16 trees for LN4. All samples were processed according to the dendrochronological procedure [32], including air-drying and grinding, and the ring widths were measured by a LINTAB6 with an accuracy of 0.01 mm. Cross-dating quality assessments and calibration were conducted using COFECHA software [33]. The standardization of the measured width sequences and the establishment of tree-ring chronology were per-

formed using ARSTAN software [34]. In particular, growth trends of tree-ring width series were removed by negative exponential or linear regression fits, and chronologies were built by a biweight robust mean method for SB1, HB3, and LN4 as well as the signal-free chronology for SX2 site. The details should be referenced in the corresponding literature [27–30]. We used standard chronology for further analysis, as it preserves more climate signals contained by tree rings [34].

2.2. Meteorological Data

According to the response characteristics of the tree-ring growth to the climate and the distance between the meteorological stations and the sampling sites, four meteorological stations, i.e., Luochuan (LC, 35°49′ N, 109°30′ E, elevation 1159.8 m), Yuanping (YP, 38°44′ N, 112°43′ E, elevation 828.2 m), Fengning (FN, 41°13′ N, 116°38′ E, elevation 661.2 m), and Chaoyang (CY, 41°33′ N, 120°27′ E, elevation 169.6 m), were selected for each chronology at sites of SB1, SX2, HB3, and LN4, respectively. The regional climate is characterized by high temperatures accompanied by high precipitation in summer and low temperatures accompanied by drier winters, which corresponds to the typical influence of the East Asian monsoon. The variations in monthly average precipitation and monthly average temperature over the observed years are shown (Figure 2). The meteorological data of the four stations show that the annual average temperature is 6.7–9.6 °C and the total annual precipitation is 447.6–617 mm. The hottest month is July, and the coldest month is January, with temperatures ranging from 22 °C to 24.8 °C and −11.2 °C to −4.6 °C, respectively. The total precipitation from July to September ranges from 289.7 mm to 341.1 mm. These data are from China Meteorological Information Center (http://data.cma.cn/) (accessed on 15 December 2020).

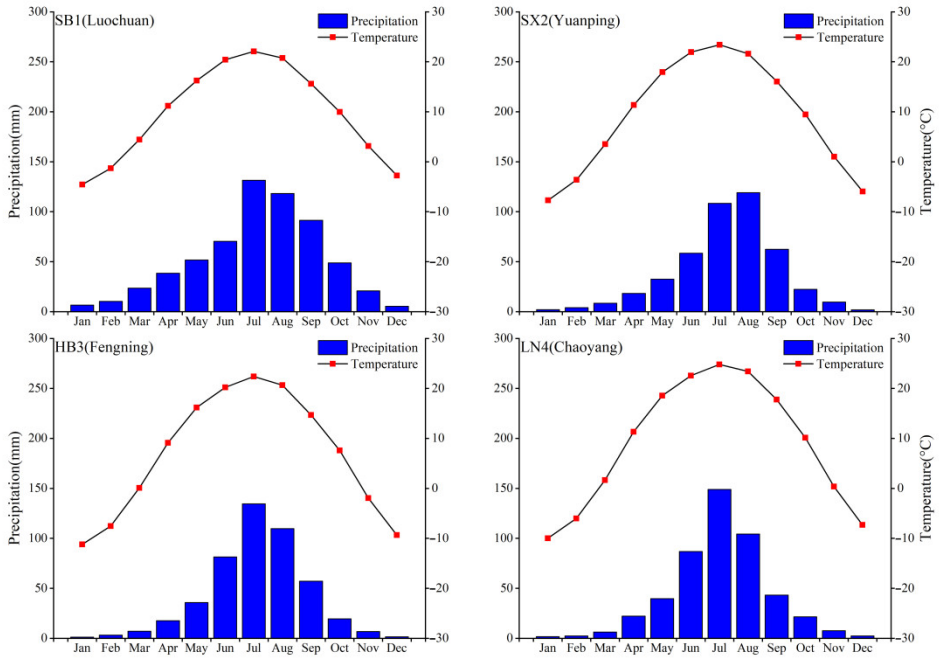

Figure 2. Variations in monthly mean temperature (red dot) and precipitation (blue bar) from the four meteorological stations used for each site.

2.3. Statistical Methods

The VS model is based on tree physiological processes and is driven by daily parameters, including temperature and precipitation [20]. This model could evaluate the daily growth rate determined by temperature (GrT), soil moisture (GrW), and solar radiation (GrE) in the growing season and reveal the distribution characteristics of the integral growth rate of the cambium (Gr). Version 1.362 of the VS-oscilloscope software

was downloaded from http://vs-genn.ru (accessed on 21 March 2022) and used [20]. Due to the lack of measured data, the appropriate parameters of physiological growth inferred from the model were determined by the differences between the actual and simulated tree-ring width chronology through iteratively debugging and comparing. The feasibility and reliability of this study were supported by previous work on *P. tabulaeformis* in Helan Mountain [25] and the Western Qinling Mountains [22]. Independent-samples t-tests were used to assess the significance of the average values of tree radial growth rates obtained from the simulated extremely wide and narrow rings. The temperatures of the onset date and cessation date of tree radial growth were calculated by a five-day moving average method [35]. Numbers from 1 to 365, corresponding to the day of the year (DOY), were assigned to the onset and cessation dates. The duration and accumulated temperatures were calculated during the period from the onset date to the cessation date [22]. Twenty-one series were calculated from 0 °C to 20 °C with intervals of 1 °C for each parameter. Correlation analyses were used to assess the relationships between the measured chronology and the simulated series, and the response intensity of the chronology to the DOY series of onset dates, cessation dates, durations, and accumulated temperatures [36].

3. Results

The comparison between the measured tree-ring chronology and the simulated sequence is shown (Figure 3). All four sampling sites showed significant positive correlations, with higher coefficients of 0.612 ($p < 0.01$) and 0.676 ($p < 0.01$) appearing at SB1 and SX2 and lower correlation coefficients of 0.394 ($p < 0.01$) and 0.466 ($p < 0.01$) appearing at HB3 and LN4.

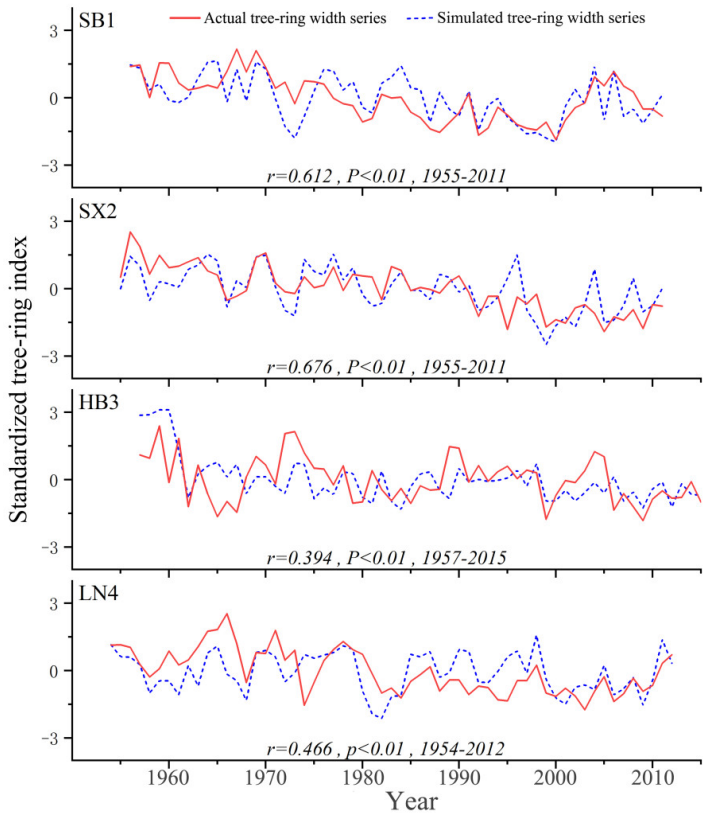

Figure 3. Comparison between the actual (red straight line) and simulated (blue dashed line) tree-ring width series (Standardized tree-ring index) during the past several decades.

According to the results of the simulated parameters (Table 1), the range of minimum temperature variation for tree growth was 4–7 °C, and the lower optimal growth temperature was in the range of 10 °C to 18 °C. The initial temperatures inferred from the four sites of SB1, SX2, HB3, and LN4 were 5 °C, 7 °C, 4 °C, and 4 °C, and the corresponding onset dates were April 6 (DOY 96), April 12 (DOY 102), April 23 (DOY 114), and April 16 (DOY 106), while the cessation dates were October 21 (DOY 296), October 24 (DOY 299), October 10 (DOY 284), and October 23 (DOY 298).

Table 1. Model parameters for the simulated tree radial growth of the four sites.

Parameter	Description (Units)	Value			
		SB1	**SX2**	**HB3**	**LN4**
T_{min}	Minimum temperature for tree growth (°C)	5	7	4	4
T_{opt1}	Lower end of range of optimal temperatures (°C)	17	18	10	14
T_{opt2}	Upper end of range of optimal temperatures (°C)	27	24	20	19
T_{max}	Maximum temperature for tree growth (°C)	30	27	33	22
W_{min}	Minimum soil moisture for tree growth (v/vs)	0.145	0.2	0.12	0.0575
W_{opt1}	Lower end of range of optimal soil moistures (v/vs)	0.25	0.45	0.15	0.225
W_{opt2}	Upper end of range of optimal soil moistures (v/vs)	0.325	0.7	0.3	0.25
W_{max}	Maximum soil moisture for tree growth (v/vs)	0.9	0.9	0.9	0.9
lr	Depth of root system (mm)	450	550	350	400
P_{max}	Maximum daily precipitation for saturated soil (mm/day)	20	20	20	40
C_1	Fraction of precipitation penetrating soil (rel. unit)	0.17	0.83	0.76	0.12
C_2	First coefficient for calculation of transpiration (mm/day)	0	0.005	0.035	0.0725
C_3	Second coefficient for calculation of transpiration (mm/day)	0.015	0.004	0.13	0.012
C_d	Coefficient for water drainage from soil (rel. unit)	0.005	0.007	0	0.004
T_g	Sum of temperature to start growth (°C)	105	91	101	93

According to the settings of the VS model, climatic factors with low relative rates are the main factors determining the radial growth of trees. Overall, the temperature-induced relative growth rate (GrT) was lower than soil-moisture-induced relative growth rate (GrW) in the early and late growing season, while GrW was lower than GrT during the main growing season, except for at LN4. Therefore, the simulated growth rates indicated that temperature and soil moisture jointly affected the radial growth of *P. tabulaeformis* at the four sites (Figure 4). The effects of temperature on radial growth occurred on the days of DOY 60–120 from March to April and DOY 270–330 from October to November, and the influences of soil moisture of DOY 120–270 on the growth of trees from May to September were particularly obvious at SB1 and SX2. Although there were differences in the simulation results of HB3 and LN4, the integral radial growth rate of *P. tabulaeformis* showed a bimodal pattern in general (Figure 4).

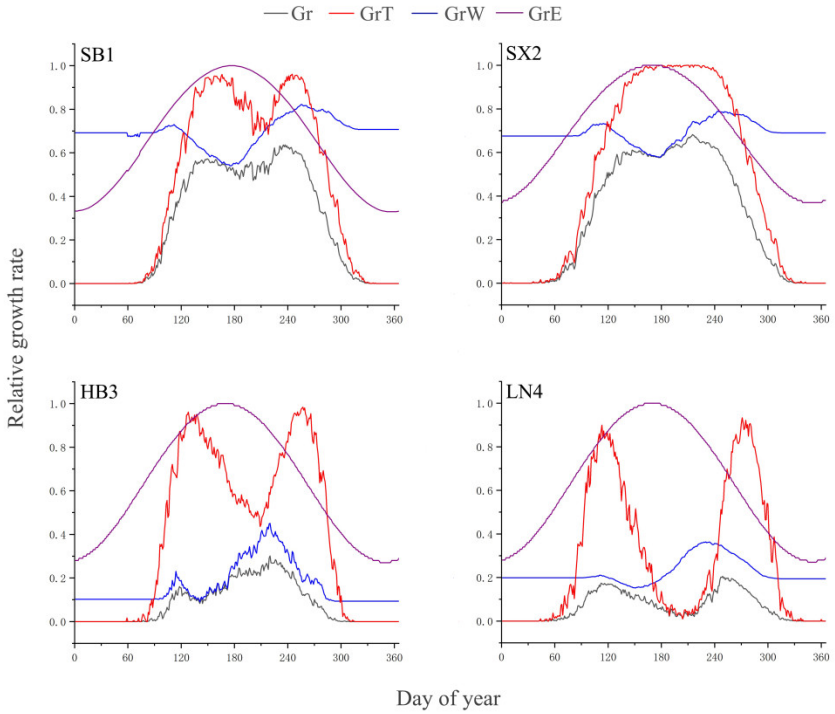

Figure 4. Simulated integral growth rate (Gr) and relative growth rates due to temperature (GrT), soil moisture (GrW), and solar irradiance (GrE) at sampling sites SB1, SX2, HB3, and LN4.

The roles of temperature and soil moisture in the radial growth of trees were judged by comparing the differences in the average radial growth rates of extremely wide and extremely narrow years. An extremely wide year is defined as more than one standard deviation from the mean of the simulated chronology; an extremely narrow year is defined as less than one standard deviation from the mean of the simulated chronology. The extremely wide years inferred from SB1, SX2, HB3, and LN4 were years 10, 7, 9, and 11, respectively, while the extremely narrow years were years 9, 10, 7, and 12, respectively (Table 2).

Table 2. Years of extremely wide rings and narrow rings.

Site	Average Value	Wide Rings (Value/Year)	Narrow Rings (Value/Year)
SB1	0.98 ± 0.24	1.32 (1956), 1.33 (1957), 1.36 (1959), 1.35 (1960), 1.26 (1966), 1.50 (1967), 1.26 (1968), 1.49 (1969), 1.31 (1970), 1.26 (2006)	0.72 (1980), 0.64 (1987), 0.61 (1988), 0.71 (1989), 0.57 (1992), 0.65 (1993), 0.69 (1996), 0.65 (1997), 0.63 (1998), 0.72 (1999), 0.53 (2000)
SX2	0.92 ± 0.32	1.74 (1956), 1.53 (1957), 1.40 (1959), 1.24 (1961), 1.31 (1962), 1.37 (1963), 1.37 (1969), 1.44 (1970), 1.24 (1983)	0.52 (1992), 0.34 (1995), 0.37 (1999), 0.48 (2000), 0.42 (2001), 0.56 (2004), 0.30 (2005), 0.51 (2006), 0.46 (2007), 0.35 (2009)
HB3	0.93 ± 0.30	1.48 (1957), 1.41 (1958), 1.68 (1959), 1.25 (1972), 1.50 (2004), 1.28 (2010), 1.66 (2013), 1.58 (2014)	0.63 (1962), 0.56 (1964), 0.23 (1967), 0.29 (1983), 0.61 (1984), 0.41 (1985), 0.42 (1999)
LN4	0.94 ± 0.38	1.37 (1954), 1.38 (1955), 1.34 (1956), 1.35 (1963), 1.62 (1964), 1.64 (1965), 1.92 (1966), 1.40 (1967), 1.63 (1971), 1.44 (1978)	0.34 (1974), 0.55 (1982), 0.47 (1984), 0.53 (1991), 0.43 (1994), 0.41 (1995), 0.55 (1999), 0.49 (2000), 0.50 (2002), 0.26 (2003), 0.40 (2006), 0.54 (2007)

The variations in the simulated mean relative growth rates related to soil moisture (GrW) and temperature (GrT) as well as the mean integral growth rate (Gr) from extremely wide years and narrow years in a calendar year are shown (Figure 5). The independent-samples t-test found that the average value of the relative growth rate related to soil moisture (GrW) in the main growing seasons (May–September) from extremely wide-year rings and narrow-year rings at SB1, SX2, HB3, and LN4 all showed significant differences ($p < 0.01$). The average growth rates for wide years were 0.867, 0.899, 0.531, and 0.328, and the average growth rates for extreme narrow years were 0.495, 0.517, 0.159, and 0.222. None of the average values of the relative growth rate related to temperature (GrT) showed significant differences ($p > 0.05$). The average values of wide years were 0.920, 0.803, 0.757, and 0.380, and the average growth rates of narrow years were 0.937, 0.778, 0.732, and 0.318. Significant differences in the average values existed in the integral growth rate (Gr) among the four sites ($p < 0.01$).

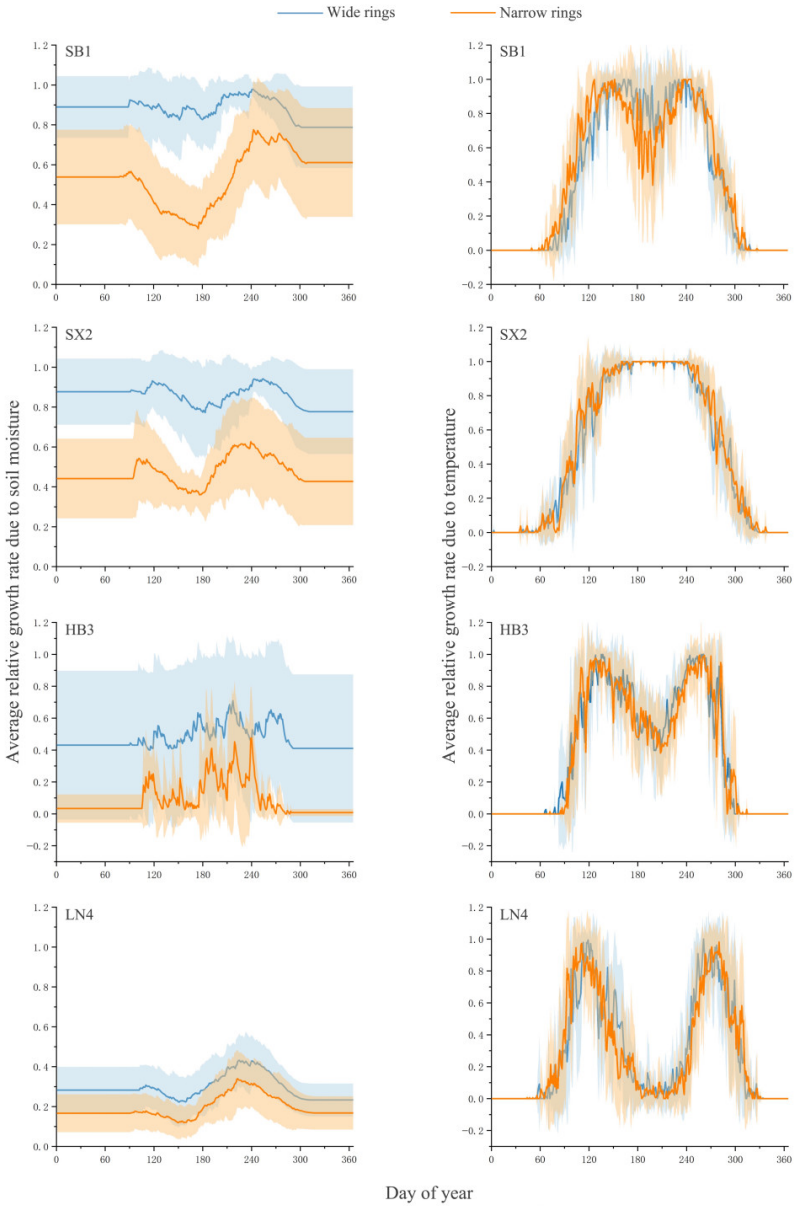

Figure 5. Comparison of the average growth rate in extremely wide and narrow rings years, as determined by temperature and soil moisture.

Correlations between the DOY series of onset date, cessation date, length of duration, and accumulated temperatures calculated from five-day moving averages of temperature parameters and tree-ring series are displayed (Figure 6). No common response temperature thresholds were found for the four sampling sites, but there were significant negative correlations ($p < 0.05$) of the DOY of the onset date and the accumulated temperature with the tree-ring chronology of SB1, SX2, HB3, and LN4. In particular, SX2 was significantly negatively correlated with the accumulated temperatures from 0 °C to 20 °C ($p < 0.05$).

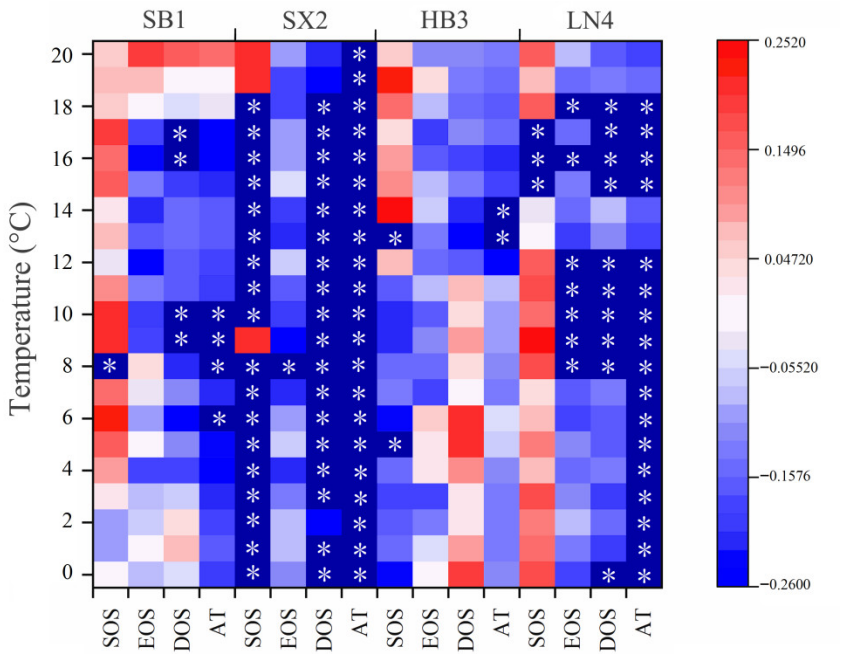

Figure 6. Correlations between tree-ring width series and the DOY series of onset date, cessation date, duration, and accumulated temperatures from each site and corresponding meteorological station.

4. Discussion

The significant correlations and consistent fluctuation characteristics indicated that the VS model was suitable for the study of the radial growth process of *P. tabulaeformis* in a wide range (Figures 3 and 4). Previous simulated results of the same species have been carried out in the eastern part of Northwest China, such as the West Qinling Mountains [22], Helan Mountains [23–25,37], and Taiheshan Mountains [22]. Our study addressed the gap in the VS simulation study of *P. tabulaeformis* in the eastern region of northern China.

The minimum temperature is associated with cell differentiation activity and is therefore considered an important limiting factor for tree growth [38]. The threshold of the daily minimum temperature of conifers in Europe and North America is 4–5 °C [39]. The initial minimum temperatures of three sampling sites at SB1, HB3, and LN4 were 5 °C, 4 °C, and 4 °C, which was in line with the threshold range mentioned above. However, the initial minimum temperature of 7 °C at SX2 reflected the differences of trees growing in diverse environmental conditions. The initial temperatures of *P. tabulaeformis* at two sites in the West Qinling Mountains were 9 °C and 12 °C, respectively [22]. Another two simulated results of the same tree species showed that the initial temperature was 7.7 °C in the Hasi Mountains [24] and 6.2 °C in the Helan Mountains [23]. A recent observational and simulated study found that the minimum air temperature strongly limited the xylem growth of *Abies georgei* at the upper tree line on the southeastern Tibetan Plateau [38]. They reported that the minimum temperature threshold was 0.7 °C,

and the best result of the VS model simulation appeared at 0.9 °C. Other tree species also showed different minimum temperatures. For example, the minimum temperature of *Juniperus przewalskii* in Northwest China is 3 °C [40], and a 6 °C minimum temperature for *Pinus sylvestris* was observed in Northeast China [41]. Therefore, differences in the minimum temperatures affecting radial growth may reflect a tree's ability to adapt to specific environments.

Although there are differences in the fluctuation characteristics, the bimodal pattern of the integral growth rates at the four sites could reflect the seasonal features of temperature and precipitation to a certain extent, especially at SB1, SX2, and LN4. One peak at the beginning of the growing season occurred in April–May, with the other one in August–September in the middle and late growing season, and the growth rate decreased into a trough in June–July (Figure 4).

High temperature coincides with more precipitation during the strong summer monsoon period, but the increasing evapotranspiration caused by high temperature in the same interval tends to induce drought stress due to the increased soil moisture deficit and therefore inhibits the growth rate of trees. The bimodal growth pattern is a response to the hydrothermal configuration of the East Asian summer monsoon on a regional scale (Figure 4). Similar bimodal patterns of the integral growth rate were shown in the simulation results of *P. tabulaeformis* in the Western Qinling [22] and Helan Mountains [23,25] at the northwestern edge of the Asian monsoon region as well as those obtained from the composite chronology of *P. tabulaeformis* and *Pinus armandii* in the Huashan Mountains to the south of SB1 [42,43]. However, the higher growth rates peaked in August–September in the current study area and May–June in the northwest of China. An observational study on the radial growth of *Platycladus orientalis* in a semi-arid area in North China found that the maximum growth rate of this conifer species occurred in August and was associated with high temperature and humidity when the availability of soil water was most suitable for the growth needs of the trees [44]. They assumed that the reasonable explanation should be attributed to the adaptability of *P. orientalis* to the local environment of the continental monsoon climate [44]. The average precipitation in August and September at the four stations is obviously higher than that in April and May (Figure 2), which supports the hypothesis demonstrated in this study area to a certain extent because the above study area was located between SX2 and HB3 (Figure 1).

Compared with the SB1 and SX2 results, there were differences in the integral growth rate simulated by HB3 and the relative growth rates related to temperature simulated by LN4. The meteorological data of Fengning station show that the average temperature in May is 15 °C, while the precipitation in May is about 40 mm (Figure 2). The spring drought stress induced by high temperature and little rainfall causes the trough in the integral growth rate of HB3 to appear in May. The same hydroclimatic conditions and radial growth rate of trees were observed in May, including precipitation, soil moisture, maximum temperature, average temperature, and minimum temperature [44]. Meanwhile, the chronology measured at HB3 was significantly negatively correlated with the average temperature in May and negatively correlated with the precipitation in May [29]. These correlation results support the response of tree growth to the climate mentioned above [29].

The relative growth rates related to temperature simulated by LN4 were lower than that related to soil moisture in July, which did not match with the result of the VS model, which indicated that the humidity condition was the main limiting factor for tree radial growth. Similar results were obtained in another *P. tabulaeformis* simulation study [45], and the specific mechanism of interaction remains to be studied in the future. In fact, the LN4 chronology was significantly positively correlated with the scPDSI from October of the previous year to September of the current year, including the scPDSI in July, and the response of growth to climate indicates that the moisture condition is the key limiting factor for tree radial growth [30].

Recently, the results of *P. tabulaeformis* microcores in the eastern subhumid area close to LN4 found that a higher radial growth rate peak of the bimodal pattern appeared in May during the main period of earlywood formation [46]. Another monitored study of *P. tabulaeformis* in the Helan Mountains found that the lower radial growth rate of trees caused by the severe drought event in June was obviously increased in August due to more rainfall [47]. The precipitation distribution in the growing season plays an important role in the radial growth of trees [48,49]. The extreme moisture limitation even caused the radial growth of *P. tabulaeformis* to appear unimodal, and the peak appeared in August in the late growing season [24]. The strongly positive response of the integral growth rate to the heavy rainfall event was also observed in August [37] in the Helan Mountains. Considering the wide range of the agro-pastoral transition zone in northern China and the diverse stand environment, the representativeness of the bimodal patterns obtained from the four sites in current study still needs to be confirmed through more field observations and monitoring analyses on the cell scale.

The variability values in the relative growth rates (GrW and GrT) induced by soil moisture and temperature in extreme wet and dry years were different (Figure 5). The average values of the relative growth rates affected by humidity were significantly different ($p < 0.01$), while no significant differences occurred at the average values of the rates affected by temperature ($p > 0.05$). These results confirm that humidity conditions dominate the radial growth of *P. tabulaeformis*. At the same time, the differences in the relative growth rate caused by humidity in extreme dry and wet years of SB1 and SX2 were larger than those of HB3 and LN4 (Figure 5). To a certain extent, this reflects the difference in the restraint strength of humidity conditions on the growth of trees at different sites.

The correlation results of the DOY series of onset dates (SOS), cessation dates (EOS), durations (DOS), and accumulated temperatures (AT) with the tree-ring chronology indicated that there were temperature thresholds for tree growth (Figure 6). Although the values were different, the inverse correlation of the accumulated temperature confirmed the limiting effect of drought stress on the growth of *P. tabulaeformis* (Figure 6). Similar response results were also reported in research work on *P. tabulaeformis* in Northwest China [36].

It is worth noting that, compared with the previous simulation results of the Hulunbuir Sandy Land in the eastern Mongolian Plateau [41] and the Qilian Mountains in the northeastern Qinghai-Tibet Plateau [50], no divergence was found between the measured tree-ring series and the simulated ones during several recent years in our study. This indicated that the drought stress or precipitation-related soil moisture caused by the rapid warming in northern China did not exceed the limits or critical thresholds of the physiological responses of the radial growth of *P. tabulaeformis* to hydroclimate elements. However, recent emissions scenario results show that the primary risk region due to more warming and drying conditions in the future appears to be the eastern plain of the arid–humid transition zone and grasslands of the southeastern Mongolian Plateau [14], including our study areas.

5. Conclusions

Variation characteristics of the radial growth rates of *Pinus tabulaeformis* were assessed by a process-based growth model at four sites in northern China. Soil moisture availability dominates tree growth in the main growing season, and temperature affects the radial growth rate of trees in the early and late growing season. The bimodal pattern exhibited by the integral growth rate reflects the configuration of water and heat in the East Asian monsoon region to a certain extent. The main peak of the integral growth rate in the study area is different from the simulation results of the same tree species in the western monsoon marginal area. More sampling sites and field observation work are necessary to further understand the mechanism of the difference in the growth response of *P. tabulaeformis* to regional hydroclimate changes.

Author Contributions: Conceptualization, G.B. and N.L.; Data curation, G.B., N.L., Y.W. and J.S.; Formal analysis, J.S., G.B., N.L. and Q.C.; Funding acquisition, G.B. and N.L.; Investigation, J.S., G.B., N.L. and Q.C.; Methodology, G.B., N.L., Y.W. and J.S.; Project administration, G.B.; Supervision, J.S. and Y.W.; Writing—original draft, J.S., N.L. and G.B.; Writing—review and editing, J.S., N.L., Y.W., G.B. and Q.C. All authors have read and agreed to the published version of the manuscript.

Funding: This work was supported by the Shaanxi High-Level Talents Special Support Program: Regional Development Talent to Guang Bao, the Research Programs of the Baoji University of Arts and Sciences to Na Liu (209010964, 209040070), the State Key Laboratory of Loess and Quaternary Geology Open Foundation (SKLLQG2109, 2031), and the Shaanxi Province University Student Innovation and Entrepreneurship Training Project (201827034). We would like to express our most sincere appreciation to Xiulan Ma for her love and support. This work is a contribution of the Innovation Team of Hydroclimatic Change and Ecological Environment of Weihe River Basin (No. 04).

Acknowledgments: We thank Feng Chen, Qi Zhou, Junjie Niu, and Yingjun Li for their great help and support. We acknowledge the reviewers for their constructive comments to improve the manuscript.

Conflicts of Interest: The authors declare no conflict of interest.

References

1. Xu, Y.Q.; Zhou, B.T.; Yu, L.; Shi, Y.; Xu, Y. Temporal–spatial dynamic pattern of forest ecosystem service value affected by climate change in the future in China. *Acta Ecol. Sin.* **2018**, *38*, 1952–1963.
2. Karnauskas, K.B.; Donnelly, J.P.; Anchukaitis, K.J. Future freshwater stress for island populations. *Nat. Clim. Chang.* **2016**, *6*, 720–725. https://doi.org/10.1038/nclimate2987.
3. Vicente-Serrano, S.M.; Camarero, J.J.; Azorin-Molina, C. Diverse responses of forest growth to drought time-scales in the Northern Hemisphere. *Glob. Ecol. Biogeogr.* **2014**, *23*, 1019–1030. https://doi.org/10.1111/geb.12183.
4. Gao, S.; Liu, R.; Zhou, T.; Fang, W.; Yi, C.; Lu, R.; Zhao, X.; Luo, H. Dynamic responses of tree-ring growth to multiple dimensions of drought. *Glob. Chang. Biol.* **2018**, *24*, 5380–5390. https://doi.org/10.1111/gcb.14367.
5. Stovall, A.E.L.; Shugart, H.; Yang, X. Tree height explains mortality risk during an intense drought. *Nat. Commun.* **2019**, *10*, 4385. https://doi.org/10.1038/s41467-019-12380-6.
6. Choat, B.; Brodribb, T.J.; Brodersen, C.R.; Duursma, R.A.; López, R.; Medlyn, B.E. Triggers of tree mortality under drought. *Nature* **2018**, *558*, 531–539. https//doi.org/10.1038/s41586-018-0240-x.
7. Ryan, M.G. Tree mortality: Large trees losing out to drought. *Nat. Plants* **2015**, *1*, 15150. https://doi.org/10.1038/nplants.2015.150.
8. Choat, B.; Jansen, S.; Brodribb, T.J.; Cochard, H.; Delzon, S.; Bhaskar, R.; Bucci, S.J.; Feild, T.S.; Gleason, S.M.; Hacke, U.G.; et al. Global convergence in the vulnerability of forests to drought. *Nature* **2012**, *491*, 752–755. https://doi.org/10.1038/nature11688.
9. Littell, J.S.; Oneil, E.E.; McKenzie, D.; Hicke, J.A.; Lutz, J.A.; Norheim, R.A.; Elsner, M.M. Forest ecosystems, disturbance, and climatic change in Washington State, USA. *Clim. Chang.* **2010**, *102*, 129–158. https://doi.org/10.1007/s10584-010-9858-x.
10. Andreu-Hayles, L.; D'Arrigo, R.; Anchukaitis, K.J.; Beck, P.S.A.; Frank, D.; Goetz, S. Varying boreal forest response to Arctic environmental change at the Firth River, Alaska. *Environ. Res. Lett.* **2011**, *6*, 045503. https://doi.org/10.1088/1748-9326/6/4/045503.
11. Fung, I.Y.; Doney, S.C.; Lindsay, K.; John, J. Evolution of carbon sinks in a changing climate. *Proc. Natl. Acad. Sci. USA* **2005**, *102*, 11201–11206.
12. Gang, C.C.; Zhang, Y.Z.; Wang, Z.Q.; Chen, Y.Z.; Yue, Y.; Li, J.L.; Cheng, J.; Qi, J.G.; Inakwu, O. Modeling the dynamics of distribution, extent, and NPP of global terrestrial ecosystems in response to future climate change. *Glob. Planet. Chang.* **2017**, *148*, 153–165.
13. Yin, Y.; Tang, Q.; Wang, L.; Liu, X. Risk and contributing factors of ecosystem shifts over naturally vegetated land under climate change in China. *Sci. Rep.* **2016**, *6*, 20905. https://doi.org/10.1038/srep20905.
14. Yin, Y.; Ma, D.; Deng, H.; Wu, S. Climate change risk assessment of ecosystem productivity in the arid/humid transition zone of northern China. *Acta Geogr. Sin.* **2021**, *76*, 1605–1617.
15. Wang, L.; Chen, W.; Huang, G.; Zeng, G. Changes of the transitional climate zone in East Asia: Past and future. *Clim. Dyn.* **2016**, *49*, 1463–1477. https://doi.org/10.1007/s00382-016-3400-4.
16. Shi, W.; Liu, Y.; Shi, X. Development of quantitative methods for detecting climate contributions to boundary shifts in farming-pastoral ecotone of northern China. *J. Geogr. Sci.* **2017**, *27*, 1059–1071. https://doi.org/10.1007/s11442-017-1421-5.
17. Heyder, U.; Schaphoff, S.; Gerten, D.; Lucht, W. Risk of severe climate change impact on the terrestrial biosphere. *Environ. Res. Lett.* **2011**, *6*, 034036. https://doi.org/10.1088/1748-9326/6/3/034036.
18. Liu, Y.; Song, H.; Sun, C.; Song, Y.; Cai, Q.; Liu, R.; Lei, Y.; Li, Q. The 600-mm precipitation isoline distinguishes tree-ring-width responses to climate in China. *Natl. Sci. Rev.* **2018**, *6*, 359–368. https://doi.org/10.1093/nsr/nwy101.
19. Tumajer, J.; Shishov, V.V.; Ilyin, V.A.; Camarero, J.J. Intra-annual growth dynamics of Mediterranean pines and junipers determines their climatic adaptability. *Agric. For. Meteorol.* **2021**, *311*, 108685. https://doi.org/10.1016/j.agrformet.2021.108685.

20. Shishov, V.V.; Tychkov, I.I.; Popkova, M.I.; Ilyin, V.A.; Bryukhanova, M.V.; Kirdyanov, A.V. VS–oscilloscope, a new tool to parameterize tree radial growth based on climate conditions. *Dendrochronologia* **2016**, *39*, 42–50. https://doi.org/10.1016/j.dendro.2015.10.001.
21. Yang, B.; He, M.; Shishov, V.; Tychkov, I.; Vaganov, E.; Rossi, S.; Ljungqvist, F.C.; Bräuning, A.; Grießinger, J. New perspective on spring vegetation phenology and global climate change based on Tibetan Plateau tree-ring data. *Proc. Natl. Acad. Sci. USA* **2017**, *114*, 6966–6971. https://doi.org/10.1073/pnas.1616608114.
22. Wu, M.; Liu, N.; Bao, G.; Gao, J. Climatic factors of radial growth of *Pinus tabulaeformis* in eastern Gansu, northwest China based on Vaganov–Shashkin model. *Geogr. Ann. Ser. A Phys. Geogr.* **2020**, *102*, 196–208. https://doi.org/10.1080/04353676.2020.1763632.
23. Zeng, X.; Wei, C.; Liu, X.; Zhang, L. Qinghai spruce (*Picea crassifolia*) and Chinese pine (*Pinus tabuliformis*) show high vulnerability and similar resilience to early-growing-season drought in the Helan Mountains, China. *Ecol. Indic.* **2019**, *110*, 105871. https://doi.org/10.1016/j.ecolind.2019.105871.
24. He, M.; Yang, B.; Rossi, S.; Bräuning, A.; Shishov, V.; Kang, S. Simulated and predicted responses of tree stem radial growth to climate change—A case study in semi-arid north central China. *Dendrochronologia* **2019**, *58*, 125632. https://doi.org/10.1016/j.dendro.2019.125632.
25. Shi, J.; Liu, Y.; Vaganov, E.A.; Li, J.; Cai, Q. Statistical and process-based modeling analyses of tree growth response to climate in semi-arid area of north central China: A case study of *Pinus tabulaeformis*. *J. Geophys. Res. Earth Surf.* **2008**, *113*, G01026. https://doi.org/10.1029/2007jg000547.
26. Zhao, W.; Wei, Z.G.; Zheng, Z.Y.; Dong, W.J. Surface temperature and precipitation variation of pastoral transitional zone in Northern China during 1964–2013. *Plateau Meteorol.* **2016**, *35*, 979–988.
27. Chen, F.; Yuan, Y.J.; Zhang, R.B.; Qin, L. A tree–ring based drought reconstruction (AD 1760–2010) for the Loess Plateau and its possible driving mechanisms. *Glob. Planet. Chang.* **2014**, *122*, 82–88.
28. Li, Y.J.; Wang, S.Y.; Niu, J.J.; Fang, K.Y.; Chao, Y.; Li, X.L.; Li, Y.H. Tree–ring–based reconstruction of drought variability (1792–2011) in the middle reaches of the Fen River, North China. *Dendrochronologia* **2016**, *40*, 1–11.
29. Wang, Y.C.; Liu, Y.; Zhang, H.F.; Wang, H.; Guo, J.L.; Zhang, E.L.; Wang, J.; Li, X. Temperature variability inferred from tree–ring records in Weichang region, China, and its teleconnection with large–scale climate forcing. *Clim. Dyn.* **2019**, *52*, 1533–1545.
30. Liu, N.; Bao, G.; Bao, M. Response Characteristics of Chinese Pine (*Pinus tabulaeformis* Carr.) Radial Growth to Climate and Drought Variability Reconstruction in Western Liaoning, Northeast China. *Forests* **2019**, *10*, 752. https://doi.org/10.3390/f10090752.
31. Cai, Q.; Liu, Y.; Fang, C.; Xie, M.; Zhang, H.; Li, Q.; Song, H.; Sun, C.; Liu, R.; Di, T.; et al. Insight into spatial-temporal patterns of hydroclimate change on the Chinese Loess Plateau over the past 250 years, using new evidence from tree rings. *Sci. Total Environ.* **2022**, *850*, 157960. https://doi.org/10.1016/j.scitotenv.2022.157960.
32. Fritts, H.C. *Tree–Rings and Climate*; Academic Press: London, UK, 1976.
33. Holmes, R.L. Computer-assisted quality control in tree-ring dating and measurement. *Tree Ring Bull.* **1983**, *43*, 69–78.
34. Cook, E.R.; Kairiukstis, L.A. *Methods of Dendrochronology: Applications in the Environmental Sciences*; Kluwer Academic Publishers: Boston, MA, USA, 1990; 394p.
35. Wang, S.T.; Wang, B.M. *Methods for the Compilation and Statistics of Meteorological Data*; China Meteorological Press: Beijing, China, 1984.
36. Bao, G.; Liu, Y.; Liu, N.; Wang, H. Radial growth response of *Pinus tabulaeformis* to temperature during the growth season in southeastern Gansu, China. *Geogr. Ann. Ser. A Phys. Geogr.* **2020**, *102*, 185–195. https://doi.org/10.1080/04353676.2020.1774243.
37. Gao, J.; Yang, B.; He, M.; Shishov, V. Intra-annual stem radial increment patterns of Chinese pine, Helan Mountains, northern central China. *Trees* **2019**, *33*, 751–763.
38. Li, X.; Liang, E.; Gričar, J.; Rossi, S.; Čufar, K.; Ellison, A.M. Critical minimum temperature limits xylogenesis and maintains treelines on the southeastern Tibetan Plateau. *Sci. Bull.* **2017**, *62*, 804–812. https://doi.org/10.1016/j.scib.2017.04.025.
39. Rossi, S.; DesLauriers, A.; Griçar, J.; Seo, J.-W.; Rathgeber, C.B.K.; Anfodillo, T.; Morin, H.; Levanic, T.; Oven, P.; Jalkanen, R. Critical temperatures for xylogenesis in conifers of cold climates. *Glob. Ecol. Biogeogr.* **2008**, *17*, 696–707. https://doi.org/10.1111/j.1466-8238.2008.00417.x.
40. Zhang, J.; Gou, X.; Zhang, Y.; Lu, M.; Xu, X.; Zhang, F.; Liu, W.; Gao, L. Forward modeling analyses of Qilian Juniper (*Sabina przewalskii*) growth in response to climate factors in different regions of the Qilian Mountains, northwestern China. *Trees* **2015**, *30*, 175–188. https://doi.org/10.1007/s00468-015-1286-0.
41. Bao, G.; Liu, Z.Y.; Liu, N.; Wu, M.L. Simulation analysis of the radial growth characteristics of *Pinus sylvestris* var. *mongolica* in Hulunbuir Sandy Land by Vaganov–Shashkin Model. *Chin. J. Appl. Ecol.* **2021**, *32*, 3448–3458.
42. Chen, F.; Zhang, R.; Wang, H.; Qin, L.; Yuan, Y. Updatedprecipitation reconstruction (AD 1482–2012) for Huashan, north-Central China. *Theor. Appl. Climatol.* **2016**, *123*, 723–732.
43. Bao, G.; Liu, N.; Wu, M.; Liu, Z. Streamflow variability in the past four centuries for the largest tributary of the Yellow River and its teleconnection with large-scale climate forcing. *Int. J. Clim.* **2021**, *42*, 4460–4476. https://doi.org/10.1002/joc.7479.
44. Jiang, Y.; Wang, B.-Q.; Dong, M.-Y.; Huang, Y.-M.; Wang, M.-C.; Wang, B. Response of daily stem radial growth of *Platycladus orientalis* to environmental factors in a semi-arid area of North China. *Trees* **2014**, *29*, 87–96. https://doi.org/10.1007/s00468-014-1089-8.
45. Gao, J.; Bao, G.; Wu, M.L.; Liu, N. Response of radial growth of planted *Pinus tabuliformis* in western Liaoning to climatic factors. *J. Earth Environ.* **2020**, *11*, 629–638.

46. Liu, W.T.; Li, J.X.; Zhao, Y.; Han, Q.; Hou, S.; Zhang, J.Y.; Li, F.; Chen, Z.J. Effects of moisture and heat coupling on xylem growth of *Pinus tabuliformis* in Shenyang, China. *Chin. J. Appl. Ecol.* **2021**, *32*, 3468–3476.
47. Gao, J.N.; Yang, B.; Qin, C. Response of intra–annual stem radial growth to drought events, A case study of *Pinus tabuliformis* in the Helan Mountains, China. *Chin. J. Appl. Ecol.* **2021**, *32*, 3505–3511.
48. Netsvetov, M.; Prokopuk, Y.; Ivanko, I.; Kotovych, O.; Romenskyy, M. *Quercus robur* survival at the rear edge in steppe: Dendrochronological evidence. *Dendrochronologia* **2021**, *67*, 125843. https://doi.org/10.1016/j.dendro.2021.125843.
49. Putz, T.R.; Urza, A.K.; Hankin, L.E.; Bisbing, S.M. Seasonal water availability drives trait variation in isolated Basin and Range *Pinus ponderosa*. *For. Ecol. Manag.* **2021**, *488*, 119022. https://doi.org/10.1016/j.foreco.2021.119022.
50. Wang, Y.F.; Zhang, Y.X.; Gou, X.H.; Gao, L.L.; Wang, F. Climate response mechanism of radial growth of *Picea crassifolia* in low altitude area of middle Qilian Mountains. *Acta Ecol. Sin.* **2020**, *40*, 161–169.